Multiple-Century Response of a Coupled Ocean–Atmosphere Model to an Increase of Atmospheric Carbon Dioxide

SYUKURO MANABE AND RONALD J. STOUFFER

Geophysical Fluid Dynamics Laboratory/NOAA, Princeton University, Princeton, New Jersey

(Manuscript received 10 June 1993, in final form 7 July 1993)

ABSTRACT

To speculate on the future change of climate over several centuries, three 500-year integrations of a coupled ocean–atmosphere model were performed. In addition to the standard integration in which the atmospheric concentration of carbon dioxide remains unchanged, two integrations are conducted. In one integration, the CO_2 concentration increases by 1% yr^{-1} (compounded) until it reaches four times the initial value at the 140th year and remains unchanged thereafter. In another integration, the CO_2 concentration also increases at the rate of 1% yr^{-1} until it reaches twice the initial value at the 70th year and remains unchanged thereafter.

One of the most notable features of the CO_2-quadrupling integration is the gradual disappearance of thermohaline circulations in most of the model oceans during the first 250-year period, leaving behind wind-driven cells. For example, thermohaline circulation nearly vanishes in the North Atlantic during the first 200 years of the integration. In the Weddell and Ross seas, thermohaline circulation becomes weaker and shallower, thereby reducing the rate of bottom water formation and weakening the northward flow of bottom water in the Pacific and Atlantic oceans. The weakening or near disappearance of thermohaline circulation described above is attributable mainly to the capping of the model oceans by relatively fresh water in high latitudes where the excess of precipitation over evaporation increases markedly due to the enhanced poleward moisture transport in the warmer model troposphere.

In the CO_2-doubling integration, the thermohaline circulation weakens by a factor of more than 2 in the North Atlantic during the first 150 years but almost recovers its original intensity by the 500th year. The increase and downward penetration of positive heat and temperature anomaly in low and middle latitudes of the North Atlantic helps to increase the density contrast between the sinking and rising regions, contributing to this slow recovery. The recovery is aided by the gradual increase in surface salinity that accompanies the intensification of the thermohaline circulation.

During the 500-year period of the doubling and quadrupling experiments, the global mean surface air temperature increases by about 3.5°C and 7°C, respectively. The rise of sea level due to the thermal expansion of sea water is about 1 and 1.8 m, respectively, and could be much larger if the contribution of meltwater from continental ice sheets were included. It is speculated that the two experiments described above provide a probable range of future climate change.

1. Introduction

The CO_2-induced change of climate has been the subject of many studies using general circulation models of the coupled ocean–atmosphere system (e.g., Bryan et al. 1982; Spelman and Manabe 1984; Schlesinger et al. 1985; Bryan and Spelman 1985; Bryan et al. 1988; Washington and Meehl 1989; Stouffer et al. 1989; Manabe et al. 1991, 1992; Cubasch et al. 1992). This study, recently summarized by Manabe and Stouffer (1993), is an extension of the earlier studies by Stouffer et al. and Manabe et al., which explored the response of a coupled ocean–atmosphere model to a gradual increase of atmospheric carbon dioxide. (Hereafter, these earlier studies will be referred to as SM for the convenience of identification.) By examining the multiple-century responses of the coupled model to the quadrupling and doubling of atmospheric CO_2, the present study examines the robustness of the results from the earlier work. The study also speculates on the nature of a large change of climate that may occur in the more distant future.

Stouffer and Manabe noted that the CO_2-induced warming of sea surface temperature is delayed markedly in the northern North Atlantic and the Circumpolar Ocean of the Southern Hemisphere due partly to the deep mixing of heat trapped by the increasing greenhouse gas. This study investigates whether such a delay continues when the time integration of the coupled model is extended over several centuries.

Based upon the paleo-oceanographic evidence, Broecker (1987) raised the possibility that the thermohaline circulation in the Atlantic and the rest of the world oceans may undergo an abrupt change in response to the global warming of climate. Using a cou-

Corresponding author address: Dr. Syukuro Manabe, Geophysical Fluid Dynamics Laboratory/NOAA, Princeton University, Forrestal Campus, US Route 1, P.O. Box 308, Princeton, NJ 08542.

pled ocean–atmosphere model with a sector computational domain bounded by two meridians 120° longitude apart and the equator, Bryan and Spelman (1985) showed that the thermohaline circulation in a model ocean with an idealized geography disappears in response to an abrupt quadrupling of the atmospheric carbon dioxide. In SM, it was noted that the intensity of the thermohaline circulation in the North Atlantic Ocean was weakened significantly in response to the gradual increase of atmospheric CO_2, due mainly to the capping of high-latitude oceans by relatively fresh near-surface water. The present study explores how the thermohaline circulation, as well as other features of the coupled ocean–atmosphere model, evolves as the concentration of atmospheric CO_2 gradually increases and remains four times or twice the initial value over many centuries.

2. Coupled ocean–atmosphere model

a. Model structure

The coupled ocean–atmosphere model used for this study is identical to the model described and used by Manabe et al. (1991). It is a general circulation model of oceans coupled to a general circulation model of the atmosphere. Heat and water budgets of the continental surface are included. The model has a global geography and seasonally varying insolation.

In the atmospheric component of the model, dynamic computations are performed using the so-called spectral element method in which the horizontal distributions of predicted variables are represented by a series of spherical harmonics and grid values (Orszag 1970; Gordon and Stern 1982). For the economy of computer time, the spherical harmonics consist of only 15 zonal sinusoidal waves and 15 associated Legendre functions (i.e., rhomboidal 15 resolution). There are nine finite-difference levels in the vertical. The effects of cloud, water vapor, carbon dioxide, and ozone are included in the calculations of solar and terrestrial radiation. Water vapor and precipitation are predicted in the model, but uniform CO_2 mixing ratio and zonally uniform distributions of ozone are prescribed. Overcast cloud is assumed whenever relative humidity exceeds a certain critical value. Otherwise, clear sky is prescribed.

The basic structure of the oceanic component of the model resembles the model described by Bryan and Lewis (1979). The finite-difference mesh used for the time integration of the primitive equation of motion has a spacing between grid points of 4.5° latitude and 3.7° longitude. It has 12 finite-difference levels in the vertical. In addition to the horizontal and vertical background mixing and convective overturning, the model has isopycnal mixing as discussed by Bryan (1987). For the specific choice of parameters in the formulation of subgrid-scale mixing processes, see Manabe et al. (1991). The model predicts sea ice using a simple model developed by Bryan (1969).

The atmospheric and oceanic components of the coupled model interact with each other through the exchanges of heat, water, and momentum at their interface. The water flux includes runoff of not only water but also ice from the continents. The runoff into oceans is computed assuming that it flows toward the direction of steepest descent. It is also assumed that an ice sheet does not melt and the net snow accumulation over it cannot exceed 20 cm of water equivalent, thereby preventing the significant change in the shape of an ice sheet.

For the purpose of bookkeeping, the melting rate of an ice sheet is nevertheless computed from the surface heat budget involving the fluxes of solar and terrestrial radiation, and latent and sensible heat (e.g., Manabe and Broccoli 1985). When the equilibrium temperature at the snow-free surface of an ice sheet exceeds the freezing point of water, it is assumed that surface temperature remains at the freezing point and the excess heat is used for melting the ice surface. The computation scheme is similar to what is used for estimating the rate of snowmelt by Manabe (1969).

b. Time integration

To explore the future change of climate over many centuries, three long-term integrations of the coupled model were performed varying the atmospheric CO_2 concentration as illustrated in Fig. 1. Starting from an initial condition, which is in a quasi-equilibrium state identified in section 2c, the standard time integration of the coupled model (hereafter referred to as the S integration) was performed, maintaining the normal concentration of atmospheric CO_2. In addition, two 500-year integrations were performed from two slightly different initial conditions. In one integration, referred to as the 4XC integration, the CO_2 concentration in the atmosphere increased by 1% yr^{-1} (compounded) until it reached four times the normal value at the 140th year and remained unchanged thereafter. [Following

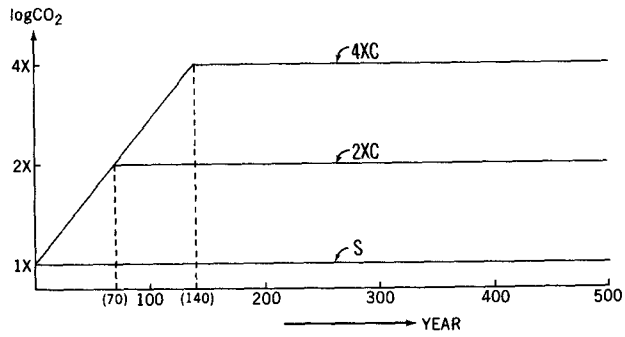

FIG. 1. Schematic of the temporal variation of the logarithm of atmospheric CO_2 concentration used in the 4XC, 2XC, and S integrations.

the "Business-as-Usual" scenario of the IPCC (1990), the total CO_2-equivalent radiative forcing of greenhouse gases other than water vapor is currently increasing at the rate of approximately 1% yr^{-1}.] The initial condition for this integration is constructed as described in section 2c. In another integration (hereafter referred to as the 2XC integration) the CO_2 concentration was increased by the rate of 1% yr^{-1} until it reached twice the normal value at the 70th year and remained unchanged thereafter. For this integration, the initial condition is extracted from the standard (S) integration but is slightly different from the condition from which both the 4XC and S integrations are initiated. The influences of the eventual quadrupling and doubling of atmospheric carbon dioxide are evaluated by computing the difference between the 4XC and S, and 2XC and S integrations, respectively. Accordingly, these two pairs of integrations will be identified as quadrupling and doubling experiments in this study. The "Business-as-Usual" scenario of the IPCC (1990) achieves a quadrupling of the CO_2 equivalent of greenhouse gases other than H_2O between 1960 A.D. and 2100 A.D. A major effort may be required to prevent the quadrupling of the CO_2 concentration in the atmosphere (see, e.g., Walker and Kasting 1992). We speculate that the eventual doubling and quadrupling of atmospheric carbon dioxide in the 2XC and 4XC integrations may provide two of the possible scenarios for a future change in the CO_2 equivalent of greenhouse gases.

c. *Initialization and flux adjustments*

When the time integration of a model starts from an initial condition that is not in equilibrium, the model climate often undergoes a rapid drift toward the state of equilibrium. For example, Manabe and Stouffer (1988) noted such a drift in the time integration of their coupled model, eventually yielding an unrealistic state characterized by an intense halocline in high latitudes and the absence of thermohaline overturning in the North Atlantic. Such a drift could distort the CO_2-induced, time-dependent response of the coupled model, which is the subject of the present study. Thus, it is highly desirable to minimize the initial drift of the model climate.

To reduce the drift of the model climate from a realistic initial condition, which is close to the state of equilibrium, the fluxes of both heat and water at the ocean–atmosphere interface are adjusted by amounts that vary seasonally and geographically. However, these adjustments, determined by the procedures described below, do not change from one year to the next and are independent of the magnitudes of the anomalies in temperature and salinity at the oceanic surface. Thus, they do not explicitly affect the damping rate of these anomalies. Furthermore, the adjustments are responsible for maintaining surface temperature and salinity near the observed distributions, despite the systematic bias of the model. Thus, they allow the model state to be perturbed or fluctuate around a realistic surface condition.

The procedures of initialization and flux adjustment were discussed in detail by Manabe et al. (1991). However, they are described below in three steps for the convenience of assessing the results obtained from the present study.

1) STEP I: ATMOSPHERIC MODEL INTEGRATION

Starting from the initial condition of an isothermal and dry atmosphere at rest, the atmospheric component of the model is integrated over a period of 12 years with seasonally and geographically varying, observed sea surface temperature [compiled by Levitus (1982)] and sea ice as a lower boundary condition. The distribution of sea ice thickness used here is subjectively determined by referring to satellite and in situ observations of the concentration and thickness of sea ice, respectively. A few years after the beginning of this integration, the model atmosphere attained a quasi-steady state in which its seasonal variation nearly repeats itself. The atmospheric state reached at the end of this integration is then used as the atmospheric part of the initial condition for the 4XC integration of the fully coupled ocean–atmosphere model. For the determination of flux adjustments mentioned above, the seasonal and geographical distribution of net downward fluxes of heat and moisture at the oceanic surface are obtained by averaging over the last 10 annual cycles of the atmospheric integration. The distribution of net surface momentum flux is also computed to be used as an upper boundary condition for the oceanic integration of step II described below.

2) STEP II: OCEANIC MODEL INTEGRATION

Following the atmospheric integration described above, the oceanic component of the model is integrated for 2400 years. Surface temperature, salinity, and sea ice thickness are relaxed toward the observed values [compiled by Levitus (1982)], which vary seasonally and geographically. Here, the relaxation time is chosen to be 50 days, which is short enough to keep the surface condition close to the observed and long enough not to constrain the model ocean too stiffly and to avoid small-scale irregularity in the distribution of the implied heat exchange at oceanic surface. The surface flux of momentum, which was obtained from the step I integration of the atmospheric model and varies seasonally and geographically, is also imposed as a part of a surface boundary condition. Throughout this oceanic integration, the approach of the deeper layers of the model ocean toward the equilibrium state is accelerated as described by Bryan et al. (1975), thereby extending the effective length of time integra-

tion from 2400 years, mentioned above, to 34 000 years. There are no trends in the model oceans toward the end of this integration. The state reached through this integration is used as the oceanic part of the initial condition for the integration of the fully coupled model. The seasonal and geographical distributions of surface heat and water fluxes, implied in the relaxation toward realistic surface temperature, surface salinity, and sea ice, are determined from the last 500 years of the integration. These fluxes are used for the determinations of the surface flux adjustments as described in step III.

3) STEP III: DETERMINATIONS OF FLUX ADJUSTMENTS FOR COUPLED MODEL

The states of the atmosphere and oceans, which were reached toward the end of steps I and II, respectively, are combined to construct the initial condition for the time integration of the coupled ocean–atmosphere model used in the present study. In addition, the differences between the two sets of heat and water fluxes obtained from the atmospheric and oceanic integrations (i.e., steps I and II, respectively) are computed. In the integration of the coupled model, the interfacial fluxes of heat and water from the atmospheric component of the coupled model are modified by the amount that is equal to the difference between the two sets of fluxes mentioned above. Although the adjustments are independent of the magnitude of the anomalies of sea surface temperature and salinity, it is encouraging that the coupled model exhibits only a very small trend throughout the course of the S integration (see Fig. 2). Identical adjustments of heat and water fluxes are also performed in not only the standard but also the 4XC and 2XC integrations.

3. Global mean response

a. Surface air temperatures

Figure 2 contains the time series of global mean surface air temperature from the 4XC and 2XC integrations. For reference, the time series from the S integration is also added to the same figure. During the first 140 years of the 4XC integration when atmospheric carbon dioxide concentration increases by 1% yr^{-1}, the global mean surface air temperature increases by 5°C, at a rate of approximately 3.5°C $century^{-1}$. This rate is slightly larger than the rate of 3.0°C $century^{-1}$, which is the best estimate of the IPCC (1990) for the Business as Usual emission of greenhouse gases. After the 140th year, global mean surface air temperature increases by an additional 1.5°C despite the absence of CO_2 increase in the model atmosphere. This slow increase results partly from the very slow adjustment of sea surface temperature toward equilibrium in the northern North Atlantic and the immediate vicinity of the Antarctic continent, where the effective thermal inertia of the ocean is very large due to the deep vertical mixing of heat.

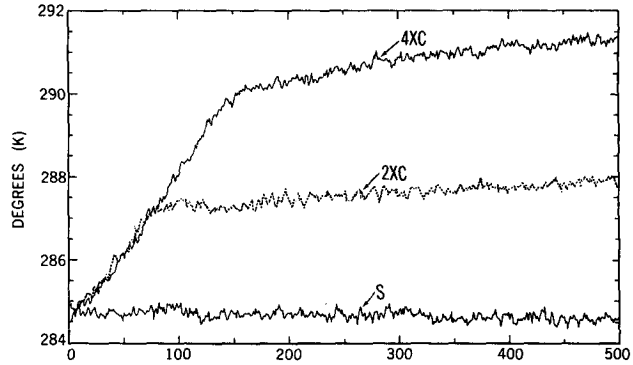

FIG. 2. Temporal variation of the global mean surface air temperature from the 4XC, 2XC, and S integrations. Units are in kelvin.

A qualitatively similar feature is evident in the time series of the 2XC integration. During the first 70 years, when atmospheric carbon dioxide increases by 1% yr^{-1}, the global mean temperature increases by 2.2°C, again at the rate of about 3.5°C $century^{-1}$ and is nearly identical to the rate during the first 140 years of the 4XC integration despite the slight difference in initial condition between the two integrations. After atmospheric carbon dioxide concentration stops increasing at the 70th year, the global mean surface air temperature increases by an additional 1°C. However, the rate of warming is about 0.2° ~ 0.25°C $century^{-1}$, which is about half the residual warming rate of 0.4° ~ 0.5°C $century^{-1}$ in the 4XC experiment. As discussed in section 4b, the vertical mixing of heat due to thermohaline circulation and convective overturning in the 4XC experiment decreases much more than in the 2XC experiment, thereby reducing faster the effective thermal inertia of oceans. Accordingly, after cessation of the increase in atmospheric CO_2, the approach of global mean surface air temperature toward the equilibrium value is faster in the 4XC than the 2XC experiment as indicated in Fig. 2.

b. Sea level

The temporal variations of the global mean sea level due to the thermal expansion of sea water are obtained for both the 4XC and 2XC experiments and are shown in Fig. 3. Although sea level is not explicitly computed in the present model, the global mean sea level rise shown here is computed separately by summing up the local change in specific volume for the entire world ocean (Bryan and Hsieh 1993).

Figure 3 indicates that, during the first few decades of the 4XC experiment, sea level rises at the rate of approximately 1 cm $decade^{-1}$. The rate increases up to about 5 cm $decade^{-1}$ by the 100th year. The sea level continues to rise at this rate until about the 180th

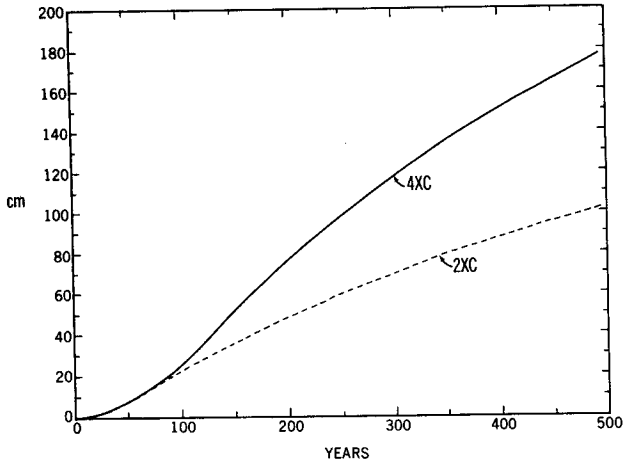

FIG. 3. Temporal variation of the global mean sea level from the 4XC and 2XC experiments. The 4XC and 2XC time series represent the difference between the 4XC and S, and 2XC and S integrations, respectively. Units are in centimeters.

year. Even after the 180th year, the rate of sea level rise is reduced only very gradually. As discussed in section 5, the gradual, downward penetration of positive temperature anomaly in the model oceans is mainly responsible for the continuous sea level rise after the 140th year when the atmospheric CO_2 stops increasing.

In the 2XC experiment, the initial rate of sea level rise is nearly identical to the initial rate in the 4XC experiment. By the 70th year when atmospheric carbon dioxide stops increasing, the rate of sea level rise reaches 3 cm decade^{-1} and stays at this value until about the 110th year when it begins to decrease very gradually. A qualitatively similar feature is indicated in the curve of sea level rise obtained by Warrick and Oerlemans [Fig. 9.8 of IPCC (1990)]. Note, however, that their result includes the contribution of meltwater from ice sheets and mountain glaciers.

Because of the downward penetration of a larger temperature anomaly, the rate of sea level rise is larger in the 4XC than the 2XC experiment even after the atmospheric CO_2 stops increasing in both experiments. Thus, the total sea level rise over the entire 500-year period of the 4XC experiment amounts to about 1.8 m and is substantially larger than the corresponding rise of about 1 m in the 2XC experiment.

Although the meltwater from continental ice sheets is not included in the computation of sea level rise mentioned above, the rate of melting at the surface of ice sheets has been estimated as described in section 2b for the sake of bookkeeping. Assuming that the meltwater does not refreeze at all in the ice sheet, sea level would rise by as much as an additional 7 m during the 500-year period of the 4XC integration, resulting in a total sea level rise of about 9 m. Even if only half of the meltwater were to eventually run off into the oceans, the total sea level rise would be about 5 m. (For the temporal variation of the meltwater from continental ice sheets, see Fig. 14 in section 4b.)

4. Thermohaline circulation

a. Temporal variation

One of the most remarkable aspects of the 4XC integration is the gradual disappearance of the thermohaline circulations in the model oceans. For example, the thermohaline circulation almost vanishes in the North Atlantic Ocean before the end of the 4XC integration (Fig. 4). It weakens rapidly during the first 140 years of the CO_2 increase, and continues to decrease after the 140th year despite the absence of the CO_2 increase until its intensity is reduced to a few Sverdrups (1 Sv $\equiv 10^6$ m^3 s^{-1}) around the 200th year. During the second half of the integration, very weak overturning is essentially confined equatorward of 45°N with practically no sinking in the northern North Atlantic (Fig. 5c). In the immediate vicinity of the Antarctic continent, the thermohaline overturning not only weakens markedly but also shifts toward the surface during the first 140 years of the 4XC integration (Figs. 5g and 5h). Although the coastal cell of thermohaline circulation reintensifies slightly after the 140th year, it is essentially confined to the top 1.5-km layer of ocean, (Fig. 5i), resulting in a marked reduction of the formation of Antarctic Bottom Water. Thus, the northward flow of the bottom water stops and the deep cell of clockwise circulation disappears in the Pacific Ocean (Fig. 5f). The reduction in the formation of the Antarctic Bottom Water (AABW) also affects deep circulation in the Atlantic sector. Although the clockwise cell of AABW in the Atlantic intensifies during the first 140 years as the upper thermohaline cell becomes shallower, it eventually disappears and the northward flow of the bottom water also stops for all practical purposes toward the end of the 4XC integration (Fig. 5c). In summary, most of the thermohaline circulations disappear in the model oceans toward the end of the 4XC integration, leaving the wind-driven, shallow cells in

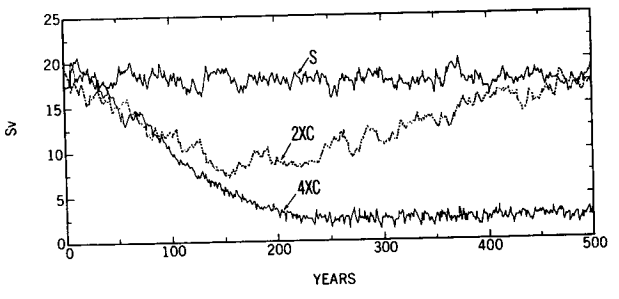

FIG. 4. Temporal variation of the intensity of the thermohaline circulation in the North Atlantic Ocean from the 4XC, 2XC, and S integrations. Here the intensity is defined as the maximum value of the streamfunction representing the meridional circulation in the North Atlantic Ocean (e.g., Fig. 5a). Units are in Sverdrups.

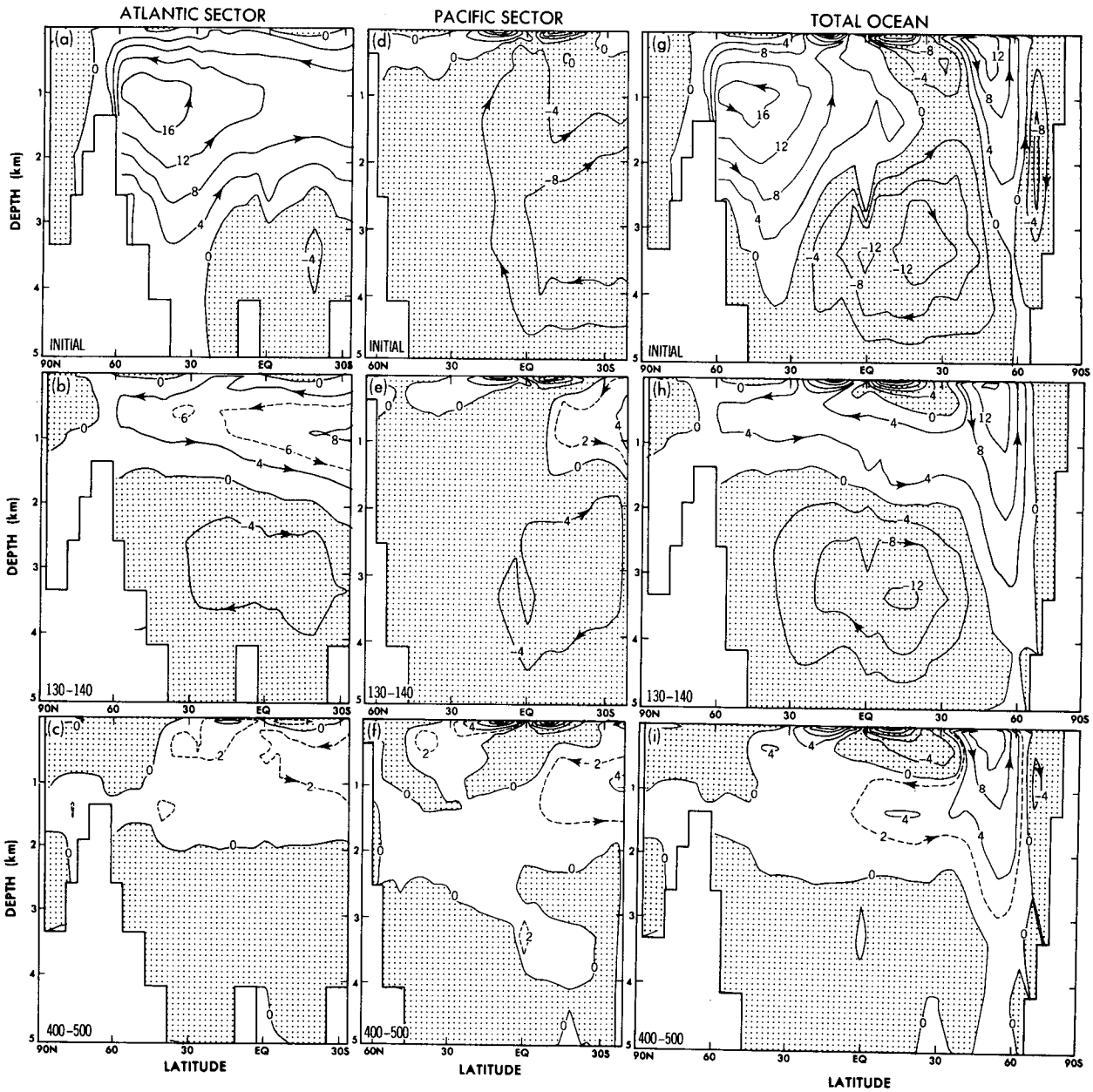

FIG. 5. Streamfunction of the meridional circulation in the Atlantic (left column, a–c), Pacific (middle column, d–f), and total oceans (right column, g–i) from the 4XC integration. Top row: initial condition. Middle row: average over 130th–150th year. Bottom row: average over 400th ~ 500th year. Units are in Sverdrups.

the subtropics of both hemispheres and the deep cell in the Circumpolar Ocean of the Southern Hemisphere. Thus, the ventilation of the deeper half of the model oceans is reduced markedly.

It is important to note here that the thermohaline circulation in the standard (S) integration maintained its initial intensity throughout the course of the integration. For example, the intensity of thermohaline circulation in the North Atlantic remains in the range of 16 ~ 19 Sv in sharp contrast to the 4XC integrations in which it is reduced to a few Sv as described earlier (Fig. 4). One notes, however, that the intensity of the thermohaline circulation fluctuates by a few Sv on a time scale of 40–50 years. For further discussion of this phenomenon, see Delworth et al. (1993).

In the 2XC integration, the thermohaline circulation also weakens in the North Atlantic during the first 70 years. After the 70th year, when atmospheric carbon dioxide ceases to increase, it continues to decrease and is eventually reduced down to less than half of its orig-

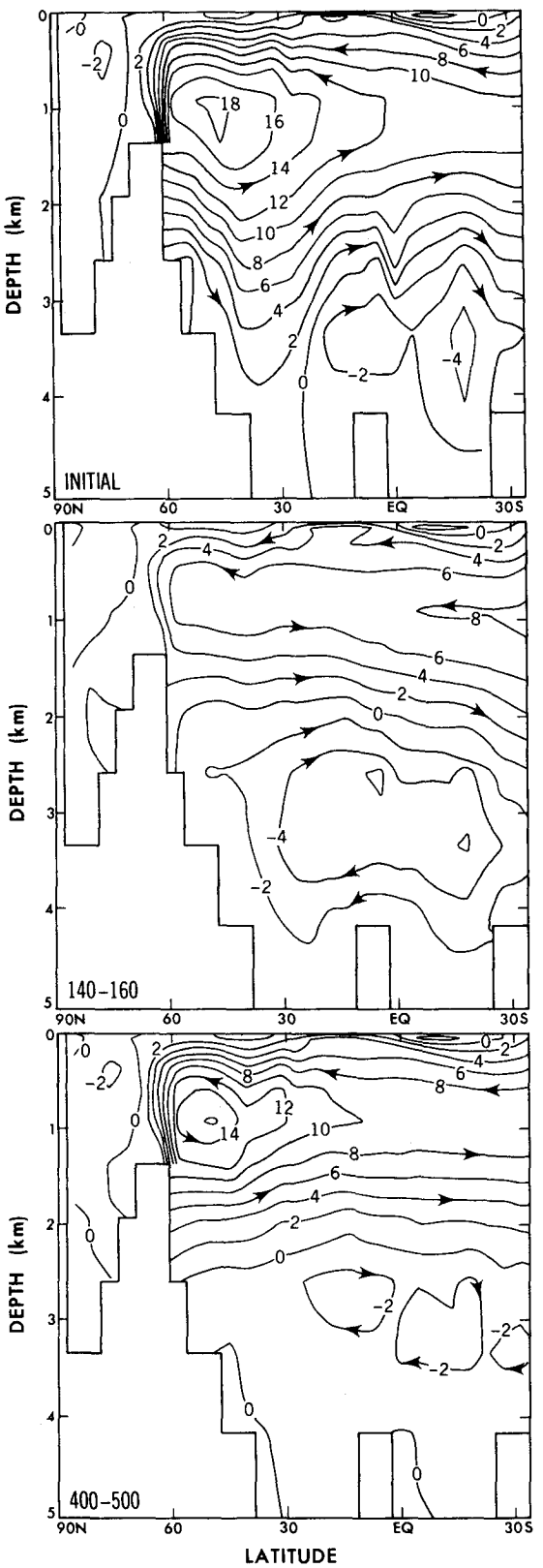

FIG. 6. Streamfunction of meridional circulation in the Atlantic Ocean from the 2XC integration. (a) Initial condition. (b) Average over 140th–160th year. (c) Average over 400th–500th year. Units are in Sverdrups.

inal intensity. However, the thermohaline circulation begins to increase very slowly around the 150th year of the integration. By the 500th year, it is almost restored to its original intensity although it does not penetrate as deeply and intensifies mostly in the North Atlantic (Fig. 6). The slow recovery in intensity after the 150th year of the 2XC integration underscores the resiliency of the circulation. It also implies that the weakening of the thermohaline circulation during the early phases of the 2XC (or 4XC) integration is not a collapse of the circulation due to instability. Instead, it represents the slow adjustment of the circulation to the evolving density structure of the model's Atlantic Ocean.

In the coastal seas near the Antarctic coast, thermohaline circulation intensity is reduced from 8 Sv down to only a few by the 160th year of the 2XC integration and it remains weak until the end of the experiment. The formation of the Antarctic Bottom Water ceases and the northward flow of the bottom water disappears altogether in the Pacific Ocean.

b. Surface flux of fresh water

It has been found that the near extinction of the thermohaline circulation described above results mainly from the capping of oceans by relatively fresh, low-density water in high latitudes. Figure 7 illustrates the changes of zonal mean salinity during the entire 500-year period of the 4XC integration. According to this figure, zonal mean surface salinity decreases in high latitudes of both hemispheres, particularly over the Arctic Ocean where the intense halocline prevents mixing between the surface and deeper layers.

The reduction of surface salinity described above is attributable to the marked increase in the supply of fresh water at the oceanic surface (i.e., the excess of precipitation over evaporation over oceans, runoff from continents, and the melting of sea ice) in high latitudes. Figure 8 compares the rates of precipitation and evaporation toward the end of the 4XC integration with the rates from the S integration. This figure indicates that in high latitudes the increase of precipitation is much larger than that of evaporation. Because of the increase in the moisture content of air that accompanies the tropospheric warming, the poleward transport of water vapor is enhanced, resulting in an increase of the excess of precipitation over evaporation (i.e., P-E) in high latitudes. The increase in (P-E), in turn, contributes directly to an increase in the supply of fresh water over oceans or, indirectly, through enhanced runoff from continents. Another source of fresh water

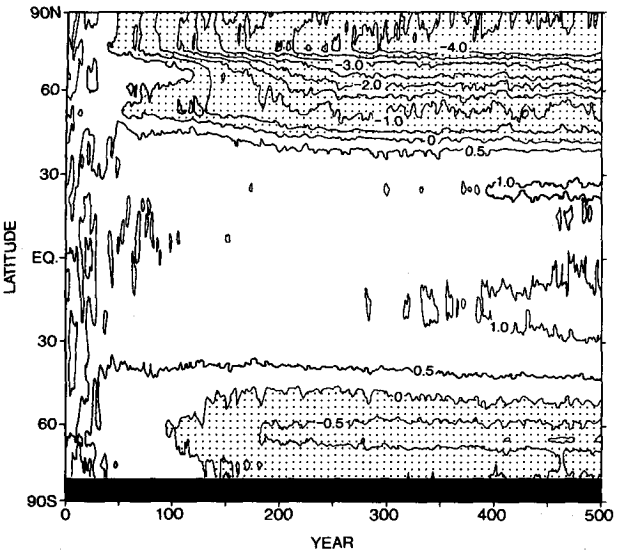

FIG. 7. The temporal variation of the latitudinal distribution of annual mean difference of surface salinity between the 4XC and S integrations. The salinity is zonally averaged over all oceans. Units are practical salinity units (psu).

in the present model is the melting of sea ice. Its magnitude, however, is relatively small.

Figure 9 illustrates, for both Atlantic and Pacific oceans, $\Delta\sigma_t$, that is, the zonal mean difference in sigma-t between the last 100-year period of the 4XC and S integrations [see, e.g., Neuman and Pierson (1966) for the definition of sigma-t]. It indicates the CO_2-induced change of density during the 4XC experiment. For the Atlantic Ocean, $\Delta\sigma_t$ is subdivided into two parts [Eq. (1b)], that is, $\Delta_S\sigma_t$ and $\Delta_T\sigma_t$, which are attributable to the changes in salinity and temperature, respectively:

$$\Delta\sigma_t = (\sigma_t)_{4XC} - (\sigma_t)_S \qquad (1a)$$

$$\sim \Delta_S\sigma_t + \Delta_T\sigma_t, \qquad (1b)$$

where

$$\Delta_S\sigma_t = \sigma_t(S_{4XC}, T_S) - \sigma_t(S_S, T_S), \qquad (2)$$

$$\Delta_T\sigma_t = \sigma_t(S_S, T_{4XC}) - \sigma_t(S_S, T_S), \qquad (3)$$

and suffixes 4XC and S indicate the 4XC and S integrations, respectively. The distributions of the zonal mean values of $\Delta_S\sigma_t$ and $\Delta_T\sigma_t$ are shown in Fig. 10.

These figures (i.e., Figs. 9 and 10) indicate that, during the course of the 4XC integration, the density of water is reduced substantially in the near-surface layer of the Atlantic Ocean poleward of 45°N due mainly to the reduction of salinity. The layer of salinity-induced, negative density change becomes deeper toward the Arctic Ocean. The development of this thick surface layer of reduced salinity described here is attributable not only to the increased supply of fresh water at the oceanic surface, but also to the weakening of the thermohaline circulation, which supplies relatively saline water to the northern North Atlantic and Norwegian seas. In contrast to the situation in high northern latitudes, the salinity-induced change of density is positive in low latitudes (i.e., 40°N ~ 40°S) of both hemispheres (Fig. 10) where water rises very slowly as a part of the thermohaline circulation in the Atlantic Ocean (Fig. 5a). This positive salinity change in the upper layer of low latitudes is attributable not only to the decrease in (P-E), but also to the reduction in the upward advection of relatively fresh water due to the weakening of the thermohaline circulation. In short, the salinity changes of opposite sign occur in high northern and low latitudes of the Atlantic Ocean. On the other hand, the temperature-induced change of density has a larger negative value in low than high latitudes (Fig. 10). The net consequence is the reduction of density difference between the sinking region of the northern North Atlantic and the slowly rising region in the rest of the Atlantic and other oceans. It contributes to the weakening and eventual disappearance of the thermohaline circulation in the Atlantic.

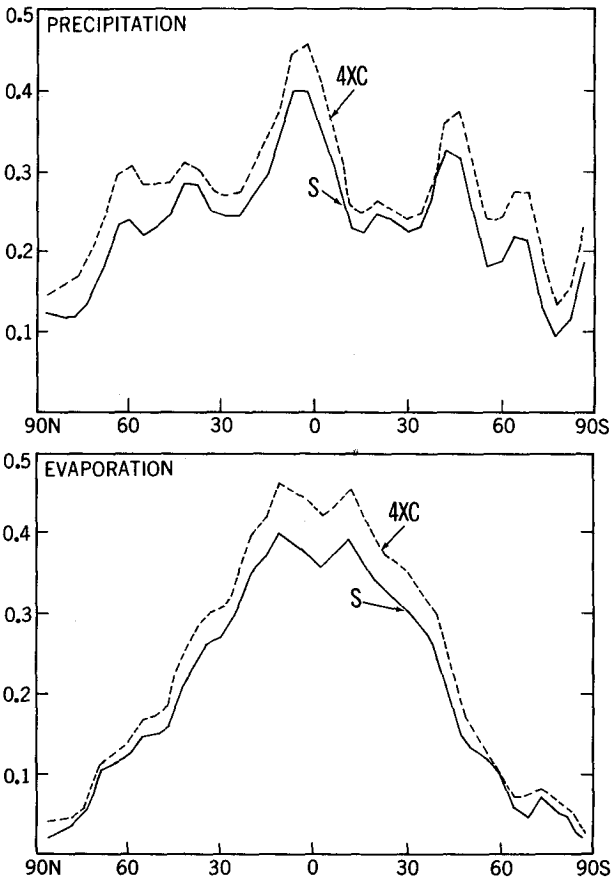

FIG. 8. The latitudinal profiles of zonally averaged, annual mean rates of precipitation (top), and evaporation (bottom) averaged over the 400th–500th-year period of the 4XC (dashed line) and S (solid line) integrations. Units are in cm day^{-1}.

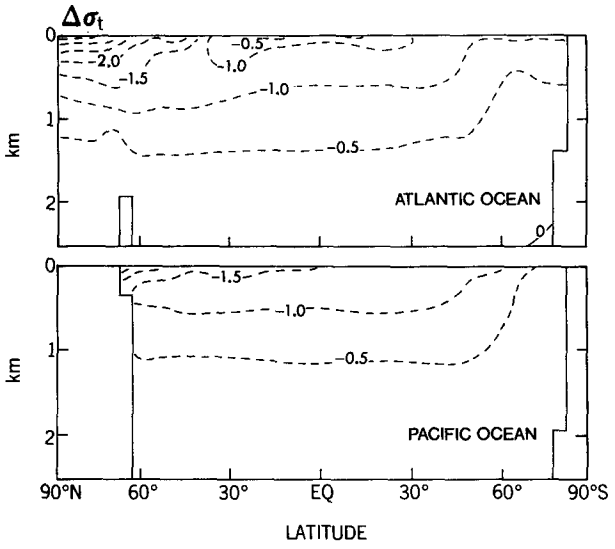

FIG. 9. The latitude–depth distribution of zonal mean difference in σ_t between the 4XC and S integrations [i.e., $\Delta\sigma_t$, see Eq. (1a)] averaged over the 400th ~ 500th-year period. Top: Atlantic Ocean. Bottom: Pacific Ocean. Note that the distribution in the deeper layers of ocean is not shown for the economy of space. The salinity is zonally averaged over all oceans. Units are practical salinity units.

A similar mechanism is involved in the weakening of the thermohaline circulation in the North Atlantic during the first 150 years of the 2XC integration. On the other hand, the slow recovery in the intensity of the circulation after the 150th year is attributable, in no small part, to the development and intensification of the subsurface positive temperature anomaly in low and middle latitudes of the North Atlantic. After the 70th year of the 2XC integration when the atmospheric CO_2 stops increasing and the rates of surface warming and freshing slow down abruptly, the thermohaline circulation continues to weaken in the Atlantic Ocean, reducing the upward advection of relatively cold water in low and middle latitudes. Thus, the subsurface layer of maximum warming develops between the equator and 45°N latitudes (Fig. 11). After the 150th year, the layer of relatively large warming extends downward and southward due mostly to isopycnal mixing (see Fig. 11). The resulting increase in the density contrast between the sinking and rising regions overshadows the salinity-induced change in meridional density contrast in the upper layer of the North Atlantic and is responsible for the slow recovery of the thermohaline circulation mentioned above.

In the 4XC integration, the temporal variation of the thermohaline circulation is significantly different from the 2XC integration described above. In the northern North Atlantic, the rate of freshwater supply continues to increase much longer than in the 2XC integration. By the 140th year when atmospheric CO_2 stops increasing, the capping by a near-surface layer of very low salinity is so effective that the formation of deep water nearly ceases in high latitudes. By the 220th year, when surface salinity stops decreasing, the thermohaline circulation becomes very weak not only in the Northern but also in the Southern Hemisphere, and the entire Atlantic gets into the state of inactive thermohaline circulation despite the substantial warming of upper oceanic layers in low latitudes. Thus, it does not recover as it does in the 2XC integration.

In the northern North Pacific and immediate vicinity of the Antarctic continent, the salinity-induced reduction of density is essentially confined to the thin surface layer in contrast to the situation in the North Atlantic. Nevertheless, the salinity reduction in the Southern Ocean appears to be large enough to weaken and make shallower the thermohaline overturning in the Weddell and Ross seas, markedly reducing the formation of the Antarctic Bottom Water as described below.

The increase of the static stability resulting from the reduction of salinity in the upper layer of oceans in high latitudes not only weakens thermohaline circulation but also drastically reduces the convective activity in the model oceans. Figure 12 illustrates the zonal mean rate of temperature change attributable to convection for both the standard (S) and the last 100-year period of the 4XC integration. This figure indicates that, in the standard experiment, convection penetrates deeply in high latitudes of the Northern Hemisphere and in the immediate vicinity of the Antarctic continent. (Although it is not shown here, convection penetrates very deeply in the northern North Atlantic and down to an intermediate depth of 1 km in the northern North Pacific.) However, convection becomes very

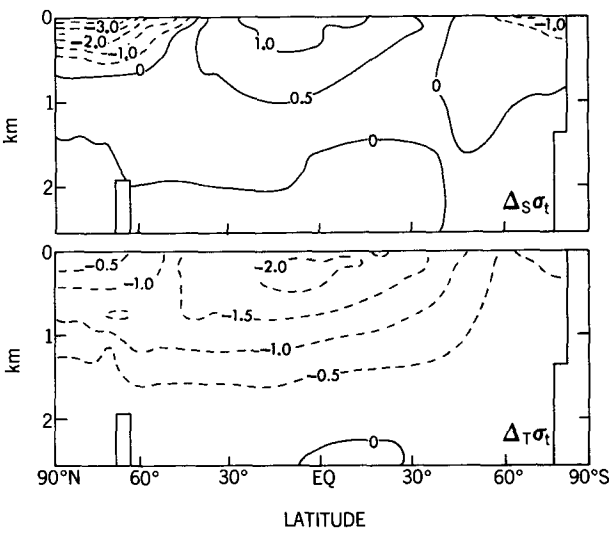

FIG. 10. The latitude–depth distribution of zonal mean values of $\Delta_S\sigma_t$ (top) and $\Delta_T\sigma_t$ (bottom) in the Atlantic Ocean averaged over the 400th–500th-year period of the 4XC experiment. See Eqs. (2) and (3) for the definition of $\Delta_S\sigma_t$ and $\Delta_T\sigma_t$, respectively. Note that the distribution in the deeper layers of ocean is not shown for economy of space. Units are in practical salinity units.

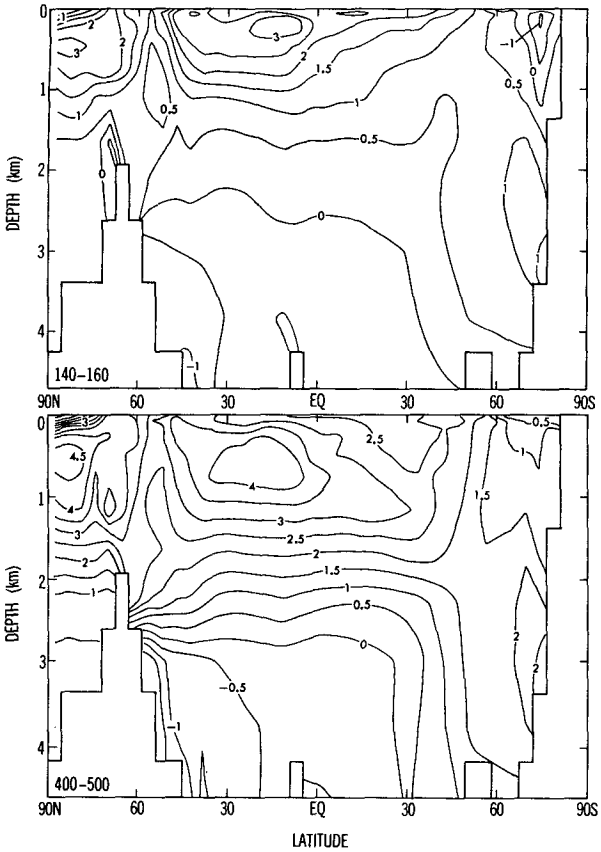

FIG. 11. Latitude–depth distribution of zonal mean difference in temperature (°C) between the 2XC and S integration for the 140th–160th-year period (top) and 400th–500th-year period (bottom).

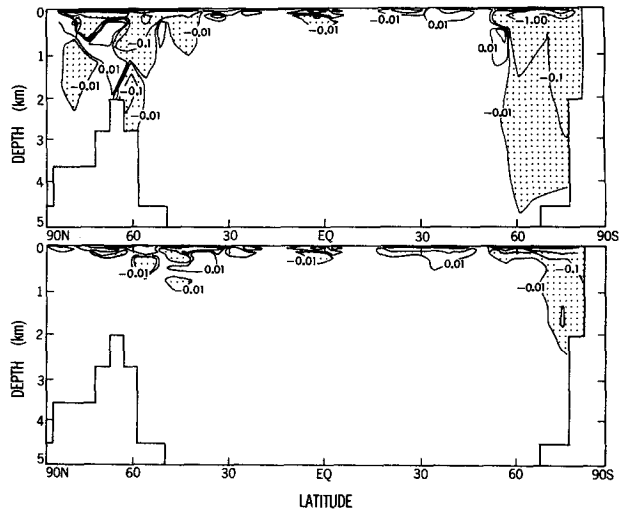

FIG. 12. Zonal mean rate of temperature change (°C 10 yr^{-1}) attributable to convection in the model oceans. Top: standard integration (0–100th year). Bottom: 4XC integration (400th–500th year).

shallow and is essentially confined to the near-surface layer of oceans toward the end of the 4XC integration, with the exception of the Ross Sea where it penetrates down to an intermediate depth. In short, the deeper half of the model oceans is no longer ventilated through either thermohaline or convective overturning. Thus, the formation of Atlantic Deep Water is terminated and that of the Antarctic Bottom Water is reduced markedly by the end of the 4XC integration.

In SM, it was noted that the present model tends to overestimate the rate of precipitation in high latitudes (Figs. 8 and A1). Recently, it has been found that this tendency is reduced substantially when the horizontal resolution of the model is doubled (from rhomboidal 15 to 30). Nevertheless, the equilibrium response experiments conducted by an atmosphere–mixed layer ocean model indicate that the change in the precipitation rate due to the doubling of atmospheric carbon dioxide is hardly different in high latitudes between the two versions of the model with the two different horizontal resolutions (i.e., rhomboidal 15 and 30). These experiments suggest that the increase in the excess of precipitation over evaporation (i.e., P-E) may not be exaggerated by the present model as speculated by Manabe et al. (1991) (see the Appendix for further details).

In addition to the sources of fresh water discussed so far, there is another potential source, that is, the melting of continental ice sheets, which is estimated separately for our information. Figure 13 compares, for the 4XC integration, the change in the rate of the meltwater supply from the Greenland ice sheet with the two components of freshwater flux that are integrated over the region northward of 50°N latitude.

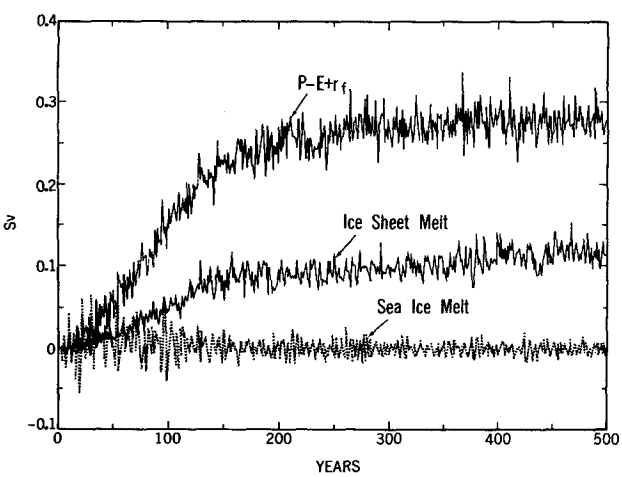

FIG. 13. The changes in the annual mean rates of 1) the excess of precipitation over evaporation (i.e., $P - E$) plus the runoff from continents and, 2) the net melting of sea ice during the 4XC integration, area integrated over the region northward of 50°N latitude. Here, precipitation (P), evaporation (E), and runoff (r_f) involve both water and ice flux. In addition, total melting at the surface of Greenland ice sheet (3) is shown for comparison. Units are in Sverdrups.

These components are 1) the excess of precipitation over evaporation (i.e., P-E) together with runoff from continents, 2) the net melting of sea ice and, 3) the meltwater from ice sheets (assuming all meltwater goes into the oceans) (shown for comparison). This figure clearly indicates that (P-E) together with runoff is the most important source of fresh water at the oceanic surface of the model, and is about 2.5 times as large as the potential contribution from the melting of the Greenland ice sheet. It could be three to five times larger if one considers that a substantial fraction of meltwater might refreeze before reaching outside an ice sheet. Nevertheless, the runoff from the melting ice sheet, if it were included, could have reduced significantly the salinity of near-surface water, thereby contributing even further to the weakening of the thermohaline circulation in the Atlantic Ocean. The contribution from the melting of sea ice, however, appears to be negligible.

The temporal variation in the rate of the meltwater supply from the Greenland ice sheet is compared with the corresponding variation from the Antarctic ice sheet (Fig. 14). The slower increase of meltwater from the Antarctic as compared with the Greenland ice sheet is attributable mainly to the relatively slow increase of sea surface temperature in the Circumpolar Ocean discussed in SM and section 6. Nevertheless, it could also have a significant effect upon the intensity of the thermohaline circulation near the Antarctic continent toward the end of the 4XC experiment as the antarctic melt rate begins to approach the Greenland rate.

As noted in section 2, the runoff of the meltwater from ice sheets into oceans and its effect upon the salinity of oceans is not incorporated in the present model. In view of our ignorance of the refreezing of meltwater and spectral truncation of ice sheet topography in the model, the estimate of ice sheet melting described above should be regarded as highly tentative. For further discussion of this issue, see Manabe and Broccoli (1985) and Broccoli and Manabe (1993).

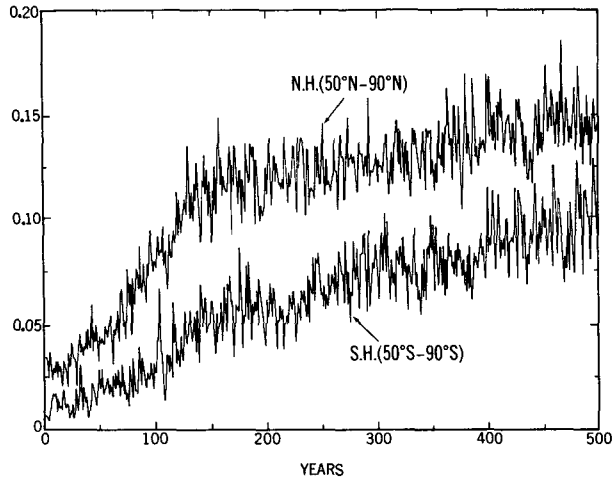

FIG. 14. Temporal variation in the annual mean rates of meltwater supply from the Greenland and Antarctic ice sheets. Units are in Sverdrups.

5. Zonal mean response

The disappearance of thermohaline circulation in the 4XC integration has a profound impact on the structure of the thermocline and the distribution of water masses in the model oceans. Firstly, one notes the marked intensification, deepening, and southward extension of the halocline in the Arctic and surrounding oceans, particularly in the Atlantic section (Fig. 15). As discussed already, these changes are attributable to not only the increased supply of fresh water, but also the marked reduction in the northward advection of saline water in the near-surface layer of oceans. Some intensification and deepening of the pycnocline are also evident in the near-surface layer close to the Antarctic continent. However, they are much less pronounced than its arctic counterpart (Fig. 15).

In general, the thermocline deepens substantially during the course of the 4XC integration. The deepening is particularly pronounced in the North Atlantic where contours of both salinity and temperature spread much more deeply (Figs. 15, 16). The marked reduction in the southward advection of relatively cold and fresh deep water by the thermohaline circulation is responsible for the deep penetrations of temperature and salinity contours in the North Atlantic. In the Pacific sector, the deepening of thermocline is much less than the Atlantic sector.

The CO_2-induced change in the zonal mean temperature of the coupled model during the 4XC integration is obtained as the difference between the last 100-year period of the 4XC and the S integration and is shown in Fig. 17. This figure clearly indicates the deep penetration of warming particularly in the ocean surrounding the Antarctic continent. In most low and middle latitudes, the warming is at a maximum in the subsurface layer of oceans. As the thermohaline circulation weakens, the upward advection of relatively cold water is reduced in low latitudes, enhancing the continued warming of the subsurface layer in the Atlantic. In addition, the abrupt cessation of the increase in atmospheric carbon dioxide around the 140th year of the 4XC integration reduced the rate of the warming of the surface layer and contributes to the formation of the subsurface maximum.

In the model atmosphere, the increase of zonal mean temperature is particularly large in the near-surface layer over the Arctic Ocean (Fig. 17) where the air–sea heat exchange is enhanced by the thinning and disappearance of sea ice. Furthermore, the albedo feedback involving sea ice and snow also amplifies the warming. In the vicinity of the Antarctic continent, the warming is much less than the Arctic due to the

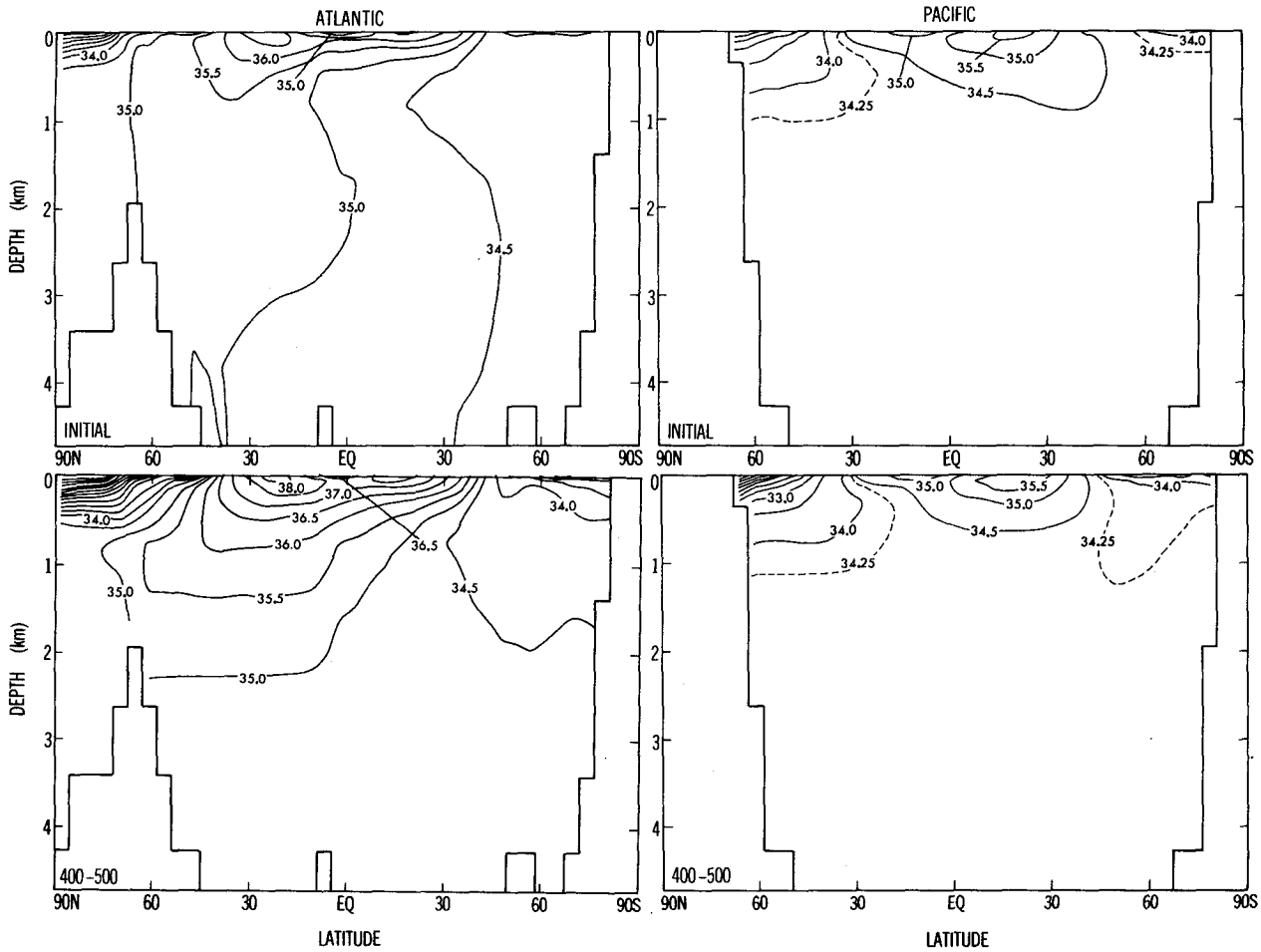

FIG. 15. Latitude–depth distribution of zonally averaged, annual mean salinity (psu) in the Atlantic (left column), and Pacific (right column) from the 4XC integration. Top row: initial condition. Bottom row: 400th–500th year average.

deep vertical mixing of heat in the Weddell and Ross seas, as discussed extensively in SM. In low latitudes, the warming is smaller than high northern latitudes in the near-surface layer of the model atmosphere and increases with increasing altitude (Fig. 17). Owing to moist convection, the vertical temperature gradient of the model troposphere in low latitudes is constrained toward the moist-adiabatic lapse rate, which decreases with increasing surface temperature. Accordingly, the tropical lapse rate of the model decreases with time, yielding the vertical warming profile described above. In the model stratosphere, temperature is reduced substantially during the course of the integration. Together with the large increase of the upper-tropospheric temperature, this cooling should result in a significant increase in the height of the tropopause.

6. Geographical structure

The geographical distributions of surface salinity in the beginning and toward the end of the 4XC integration are illustrated in Fig. 18 together with the difference between the two. This figure clearly indicates a marked reduction of surface salinity in high latitudes of both hemispheres, which results from the increased supply of fresh water, as already discussed. The reduction is particularly pronounced over the Arctic Ocean and northern North Atlantic, as discussed already. It is notable that the surface salinity over the northern North Atlantic becomes as low as the northern end of the Pacific Ocean toward the end of the 4XC integration.

In low latitudes, surface salinity increases substantially over the tropical Atlantic (Fig. 18). As noted in the preceding section, the weakening and disappearance of the thermohaline circulation results in the reduction in the upward advection of relatively fresh water, thereby increasing the near-surface salinity in low latitudes.

The geographical distributions of the increase in sea surface temperature obtained from both the 4XC and 2XC integrations are far from uniform. For example, despite the increase of atmospheric carbon dioxide, the

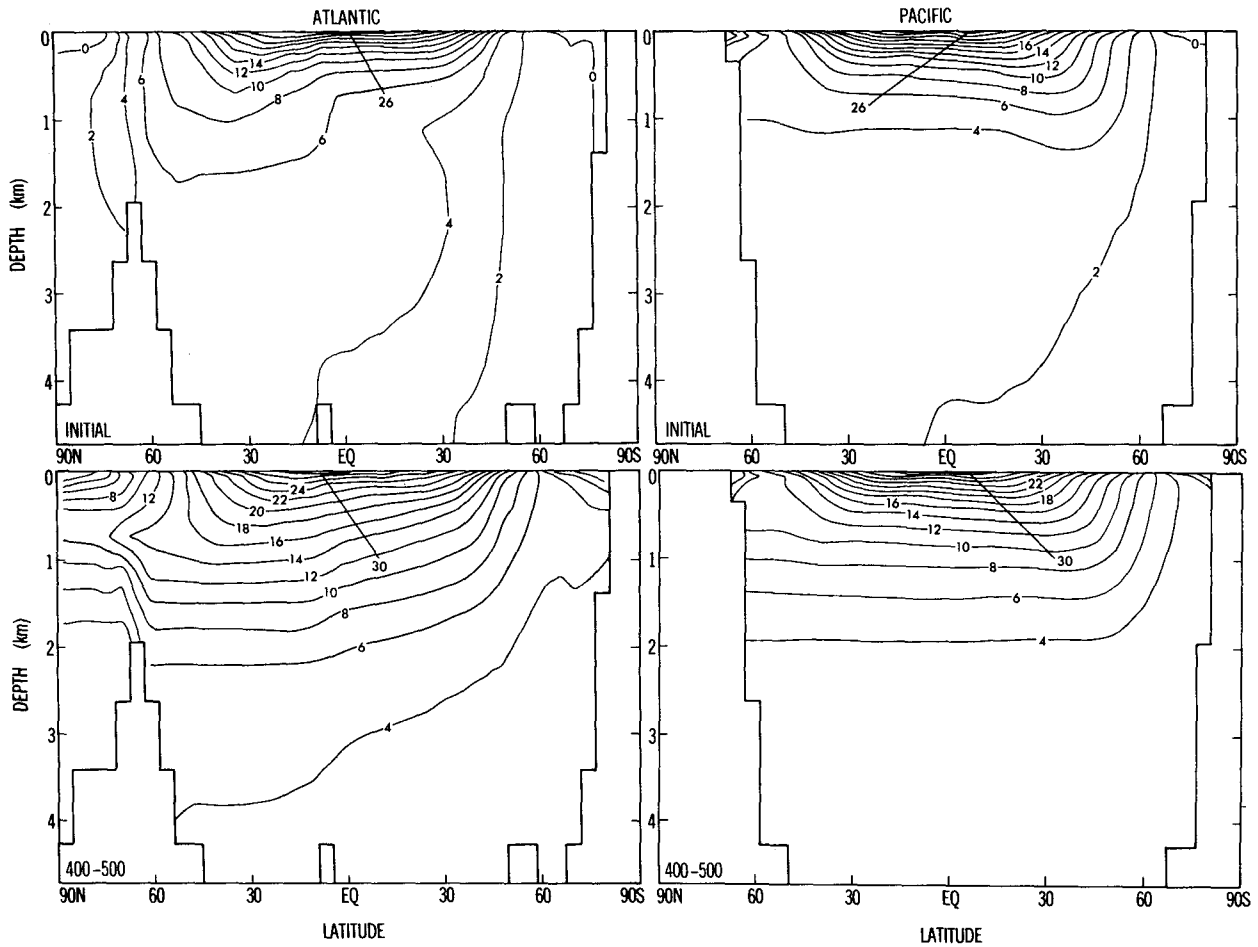

FIG. 16. Latitude–depth distribution of zonally averaged, annual mean temperature (°C) in the Atlantic (left column) and Pacific (right column) from the 4XC integration. Top row: initial condition. Bottom row: 400th–500th year average.

increase of sea surface temperature around the 140th year of the 4XC integration is close to zero in the northern North Atlantic and the vicinity of the Antarctic continent (Fig. 19a). As discussed extensively in SM, the deep vertical mixing of heat trapped by increasing atmospheric carbon dioxide helps reduce the warming of the sea surface and is partly responsible for the slow rise of sea surface temperatures in these regions. In the North Atlantic, the reduction in the northward advection of warm surface water due to the weakening of the thermohaline circulation also reduces the warming. In the Ross and Weddell seas, the capping of the surface by relatively fresh water reduces the frequency of convective overturning between the cold near-surface and slightly warmer subsurface water, resulting in the slight reduction of sea surface temperature as discussed, for example, by Manabe et al. (1990). Over the Arctic Ocean where the vertical mixing of heat is small due to the existence of an intense halocline, the increase of sea surface temperature is also small because remaining sea ice keeps surface water temperature near the freezing point. The change of sea surface temperature during the first 140-year period of the 4XC integration is qualitatively similar to the results obtained by SM. Refer to their study for further discussion of the change.

After the first 140 years of the 4XC integration, sea surface temperature continues to increase slowly in most of the model oceans despite the absence of an increase in the atmospheric carbon dioxide. The change in sea surface temperature during most of the 4XC integration is obtained as the difference between the last 100-year period of the 4XC and S integrations and is shown in Fig. 19b. In this figure, one can still identify narrow regions of no temperature change to the south of Greenland and near the Antarctic coast. Because of the marked reduction of vertical mixing, which accompanies the weakening of thermohaline circulation, the regions of relatively small sea surface temperature change become much narrower.

Figure 19b also indicates that the increase of sea surface temperature is most pronounced in the north-

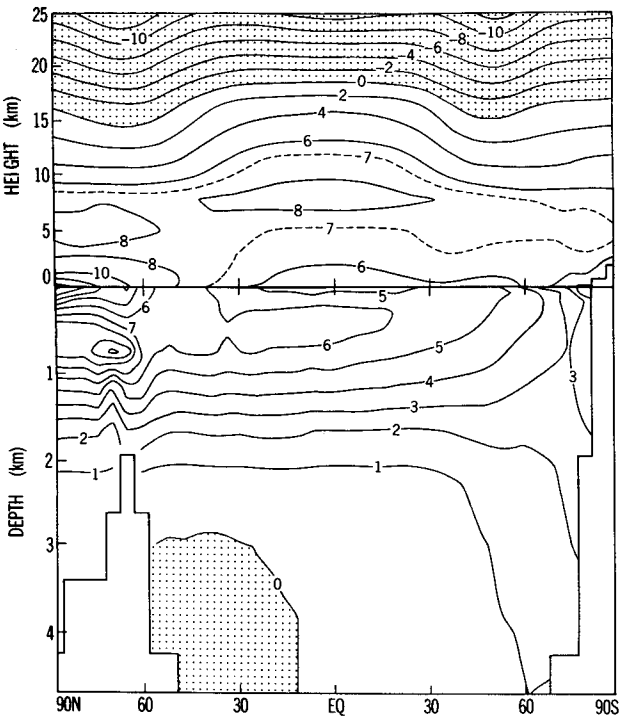

FIG. 17. Latitude–height (or depth) distribution of zonally averaged, annual mean difference in temperature (°C) between the 4XC and the S integrations averaged over the 400th–500th year period. Top: atmosphere. Bottom: ocean.

ern end of the Pacific Ocean, reaching 8°C by the end of the 4XC integration. It is also large near Greenland and in the Berents Sea. In the Southern Hemisphere the warming is relatively large in the South Atlantic around 30°S ~ 50°S.

The increase of surface air temperature is significantly different from the sea surface temperature, partly due to the existence of sea ice, which reduces the heat exchange between the water surface and overlying air. Figure 20a illustrates the distribution of the change in surface air temperature by the end of the 4XC integration. It shows that the increase of surface air temperature is about 16°C and at a maximum in high latitudes of the Northern Hemisphere. This is in sharp contrast to the relatively small increase in sea surface temperature over the Arctic Ocean. The increased heat exchange between water surface and overlying air through thinner sea ice is partly responsible for the large warming. On the other hand, the increase of surface air temperature is about 5°C ~ 6°C and is smaller than the surroundings in the Circumpolar Ocean of the Southern Hemisphere and the northern North Atlantic where the warming of sea surface is small. In general, the increase of surface air temperature in the tropics is smaller than the middle and high latitudes.

The pattern of surface air temperature change toward the end of the 2XC integration is illustrated in Fig. 20b. It is very similar to the pattern of the warming around the 70th year of the integration discussed extensively in SM. It also resembles the pattern of warming from the last 100-year period of the 4XC integration shown in Fig. 20a. However, the warming near the coast of the Antarctic continent is very small in the 2XC pattern because of the deep oceanic mixing of heat, whereas it is not as small in the 4XC case partly due to the marked reduction in the vertical mixing and the rate of formation of the Antarctic Bottom Water.

7. Concluding remarks

A coupled ocean–atmosphere model is integrated over a period of 500 years under the influence of thermal forcing that increases linearly with time until the atmospheric CO_2 concentration is quadrupled and remains unchanged to the end of the integration. It was found that the thermohaline circulation almost disappears in most of the model oceans, leaving behind wind-driven cells. For example, the thermohaline circulation nearly vanishes in the North Atlantic during the first 200-year integration. In the immediate vicinity

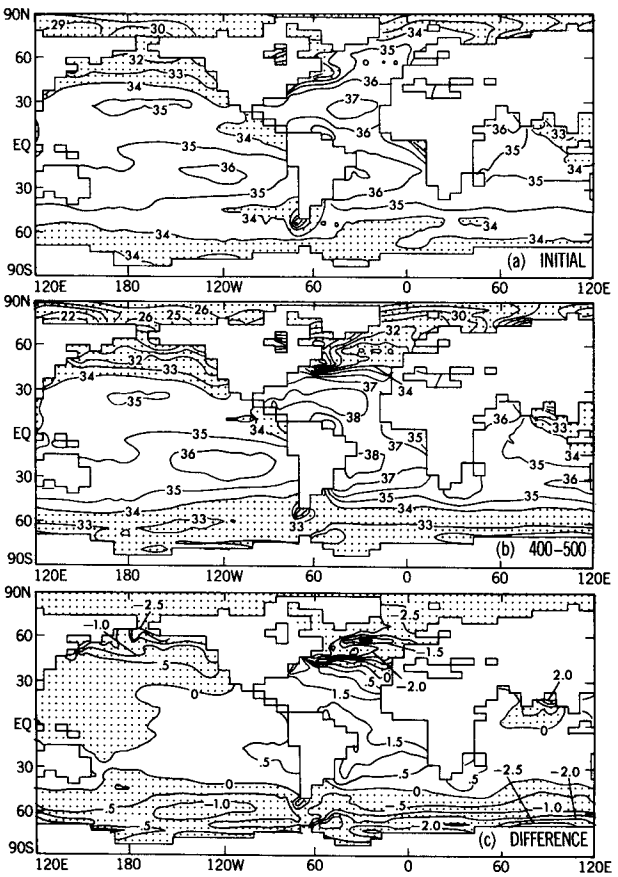

FIG. 18. Geographical distributions of annual mean surface salinity (psu) from the 4XC integration. (a) Initial condition. (b) 400th–500th year average. (c) The difference between the two.

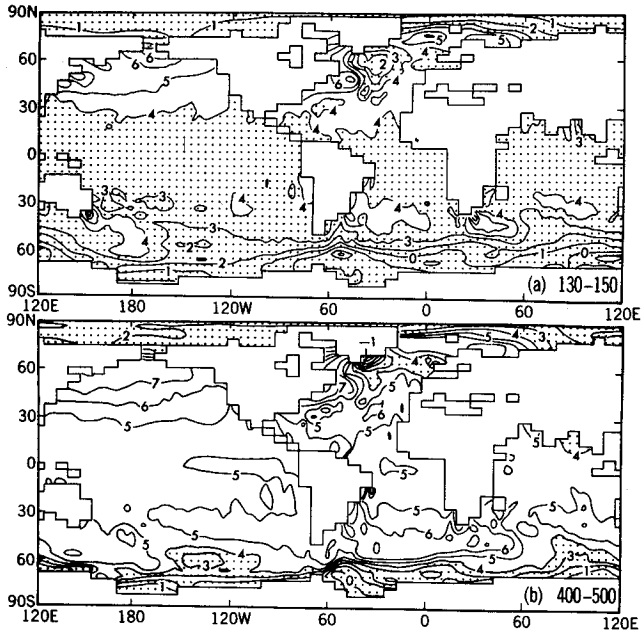

FIG. 19. Geographical distribution of the annual mean difference in sea surface temperature (°C) between (a) the 130th–150th year average and initial condition, and (b) between the 400th–500th year average and initial condition, obtained from the 4XC integration.

of the Antarctic continent, thermohaline circulation weakens and becomes shallower, markedly reducing the formation of Antarctic Bottom Water. This, in turn, weakens the northward flow of bottom water in both the Pacific and Atlantic oceans.

The near extinction of the thermohaline circulation described above is attributable mainly to the capping of oceans by relatively fresh water in high latitudes, where the supply of water to the ocean surface increases markedly. The excess of precipitation over evaporation and runoff from continents increases in high-latitude oceans due to the enhanced poleward transport of water vapor in the warmer model troposphere.

The CO_2 quadrupling integration described above is compared with another integration in which atmospheric carbon dioxide increases until it doubles and remains unchanged to the end. In this integration, the intensity of the thermohaline circulation again keeps decreasing in the North Atlantic long after the 70th year accompanied by the reduction of near-surface salinity, and it eventually is reduced down to less than half of its original intensity. However, the thermohaline circulation begins to intensify very slowly around the 150th year of the integration. Because of the reduction of the upward advection of cold water that accompanies the weakening of the thermohaline circulation, a large warming of the subsurface layer takes place in the CO_2-doubling integration between the equator and 45°N latitude. The resulting increase in the density contrast between the sinking and rising regions in the North Atlantic appears to be responsible for the gradual recovery of the thermohaline circulation by the 500th year. The recovery is aided by the gradual increase of surface salinity that accompanies the intensification of increase of surface salinity, which in turn accompanies the intensification of the thermohaline circulation.

The results from the CO_2 doubling experiment described above imply that the weakening of the thermohaline circulation in the Atlantic during the early phases of both experiments is not the collapse of the circulation due to an instability. Instead, it represents the slow adjustment of the circulation to the evolving density structure of the model's Atlantic Ocean. However, the thermohaline circulation eventually collapses in the CO_2 quadrupling integration, and does not regenerate despite the downward penetration of positive temperature anomaly in low and middle latitudes of the North Atlantic. This suggests that the state of inactive thermohaline circulation reached in the middle of the CO_2 quadrupling integration is a stable state that is distinct from that of the active circulation maintained in the early phase of both integrations. The existence of two stable equilibria in a coupled ocean–atmosphere model in the Atlantic Ocean is discussed extensively by Manabe and Stouffer (1988).

In assessing the present results, it is important to recognize that the adjustments of surface water fluxes are needed to sustain the thermohaline circulation in the Atlantic Ocean of the present model (see also Manabe and Stouffer 1988). Although the adjustments of heat and water fluxes are independent of the anom-

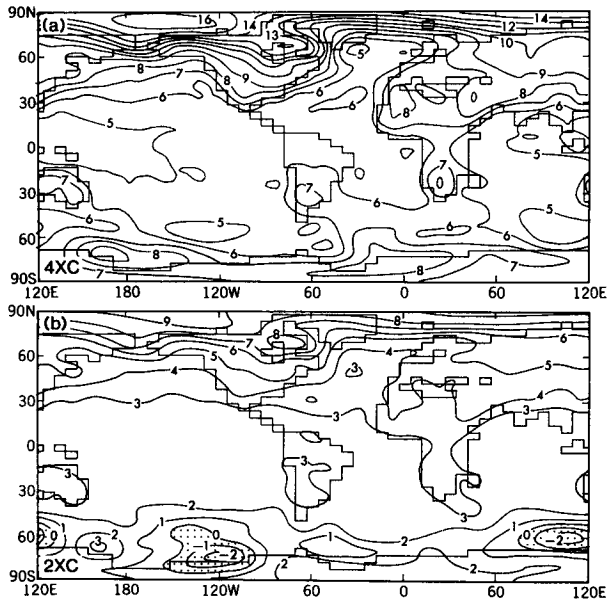

FIG. 20. Geographical distributions of the increase of annual mean surface air temperature (°C) from (a) 4XC and (b) 2XC experiments. The increase represents the difference between the 400th–500th year average of the 4XC or 2XC and 0–100th year of the S integrations.

alies of sea surface temperature and salinity and do not affect the damping rate of these anomalies, the sensitivity of the thermohaline circulation in the present coupled model could be significantly different from the actual sensitivity. Therefore, even if atmospheric carbon dioxide is quadrupled, the near disappearance of the thermohaline circulation may not be realizable in the actual ocean. On the other hand, the freshening of near-surface water due to the melting of continental ice sheets could have weakened the thermohaline circulation even more if that effect were incorporated in the model. In particular, the supply of meltwater from the Greenland Ice Sheet to the northern North Atlantic and Arctic oceans may amount to the substantial fraction of the total surface water supply to these oceans in high northern latitudes and could have a significant impact. Therefore, we take seriously the possibility of a thermohaline catastrophe such as that which occurred in the CO_2 quadrupling experiment.

By use of an ocean model with a Newtonian damping of sea surface temperature and prescribed surface water flux, Toggweiler and Samuels (1993) have shown that the surface wind stress in the Circumpolar Ocean of the Southern Hemisphere exerts strong control upon the intensity of the thermohaline circulation in the Atlantic Ocean. However, in the CO_2 quadrupling experiments conducted in the present study, the magnitude of wind stress in the Circumpolar Ocean of the Southern Hemisphere is essentially unchanged, but the thermohaline circulation disappears in the middle of the experiment. The results of the present study suggest that the water mass structure can also exert a strong influence on the intensity of the thermohaline overturning in the North Atlantic Ocean.

Based upon a set of numerical experiments that use an oceanic general circulation model with an idealized sector geography bounded by two meridians, Weaver and Sarachik (1991) noted that a stable state obtained with Newtonian damping of both surface salinity and temperature becomes unstable when the salinity condition is changed to a water flux condition. By use of a model that also has a mixed-boundary condition and an idealized geography with sector basins of the Pacific and Atlantic connected in the south by a circumpolar channel, Marotzke and Willebrand (1991) found that their "conveyor belt" thermohaline circulation transformed into an "inverse conveyor belt" solution in response to the application of surface freshwater flux anomaly of 0.05 Sv. On the other hand, thermohaline circulation in the present model shows no sign of a weakening trend during the entire 500-year period of the standard experiment. When the surface water flux (i.e., P-E) in the northern North Atlantic and Arctic oceans increases by as much as 0.15 Sv in the CO_2-doubling experiment, the intensity of thermohaline circulation is reduced to less than half of the initial level in the North Atlantic by the 150th year but almost restores its original intensity toward the end of the 500-year period. In short, the thermohaline circulation in the present, coupled ocean–atmosphere model appears to be more resilient to the increase of surface water flux in high latitudes than an ocean model with a mixed upper-boundary condition. The cause for this apparent difference has not been determined. One can speculate, however, that the damping time of sea surface temperature in ocean models may be too short in view of the observed, long-term excursion of air surface temperature with significant magnitude. Zhang et al. (1993) suggested that the thermal coupling of the model with the atmosphere is likely to inhibit the development of halocline catastrophe. It is very desirable to investigate this issue further by comparing the stability of thermohaline circulation between the coupled ocean–atmosphere model and the ocean model with mixed boundary conditions.

Toward the end of the CO_2 quadrupling integration, the thermocline becomes much deeper, particularly over the North Atlantic Ocean where the near disappearance of thermohaline circulation results in significant warming and increased salinity of deep water. The rise of surface air temperature is particularly large (i.e., 11° ~ 16°C) over the Arctic Ocean where sea ice disappears almost completely during the warmer half of the year by the end of the CO_2 quadrupling integration. On the other hand, it is 5°–8°C and is smaller than the surrounding regions in the northern North Atlantic and the Circumpolar Ocean of the Southern Hemisphere where the increase of sea surface temperature is reduced due to the vertical mixing of heat. The increase of surface air temperature over continents ranges from 7° to 10°C and is somewhat larger than over oceanic regions with the exception of the Arctic Ocean mentioned above. The temperature change described above is almost as large as the difference between the present climate and the very warm climate of the late Cretaceous (e.g., Crowly and North 1991) approximately 65–90 million years ago. In the CO_2 doubling experiment, the pattern of surface air temperature change resembles the CO_2 quadrupling experiment. Its magnitude, however, is half as large as the latter, and is even smaller in the immediate vicinity of the Antarctic continent.

In summary, this study explores the responses of a coupled model to both doubling and quadrupling of atmospheric carbon dioxide over the period of several centuries. During the entire 500-year periods of these two experiments, the global mean surface air temperature increases by almost 3.5° and 7°C, respectively. The rise of sea level due to thermal expansion of seawater is about 1 and 1.8 cm, respectively, and could be much larger if the contribution of meltwater from continental ice sheets were included. In the CO_2 quadrupling experiment, the thermal and dynamical structure of the model oceans undergoes drastic changes, such as the cessation of thermohaline circulation in most of the model oceans, and a substantial deepening

of the thermocline, especially in the North Atlantic. These changes prevent the ventilation of the deep ocean and could have a profound impact on the carbon cycle and biogeochemistry of the coupled system.

Averaged over the entire globe, the rate of increase in surface air temperature is approximately 3.5°C century^{-1} during the first 150 years of the CO_2 quadrupling integration when the atmospheric concentration of carbon dioxide increases at the rate of 1% year.$^{-1}$ This rate is approximately equal to the BAU rate of the increase of CO_2 equivalent of greenhouse gases obtained by the IPCC. This is slightly larger than the rate of 3.0°C century^{-1}, which is the best estimate by the IPCC for the BAU case. It has also been estimated that the equilibrium response of the present model to the doubling of atmospheric CO_2 is approximately 3.5°C in global mean surface air temperature. This response belongs in the upper half of the 1.5° ~ 4.5°C range of climate sensitivity estimated by the IPCC. Thus it is possible that the present model somewhat exaggerates the sensitivity of the actual climate.

According to the IPCC, the quadrupling of the CO_2 equivalent of greenhouse gases could be realized if the BAU emission of greenhouse gases continued until the end of the 21st century. Draconian measures would probably be required to prevent the CO_2 equivalent of greenhouse gases from quadrupling (e.g., Walker and Kasting 1992). Considering the possible overestimate of climate sensitivity by the present model, it may be reasonable to speculate that the CO_2 doubling and quadrupling experiments provide a probable range of future climate change. Thus, one should not discard too readily the possibility of very large long-term climate change such as that which occurred in the CO_2 quadrupling experiment.

Acknowledgments. The advice and assistance of K. Dixon were indispensible for the successful execution of the very long-term integrations of the coupled ocean–atmosphere model in the present study. J. D. Mahlman, the director of the Geophysical Fluid Dynamics Laboratory, gave whole hearted support to this project. He, J. Sarmiento and T. R. Toggweiler, and R. E. Dickinson reviewed an early version of the present paper and gave valuable comments, which significantly improved it. J. Kennedy and P. Tunison helped in the preparation of the text and figures, respectively.

APPENDIX

Precipitation and Model Resolution

This appendix evaluates how simulated precipitation and its CO_2-induced change depends upon the computational resolution of a model.

The model used for this test is an atmosphere–mixed layer ocean model. The atmospheric component of the model is identical to that of the coupled ocean–atmosphere model used in the present study. Its oceanic component is a simple mixed-layer ocean model, which is a 50-m thick slab of vertically well mixed water. The rate of heat exchange between the mixed layer and deeper layer of ocean is prescribed such that the realistic seasonal and geographical distribution of sea surface temperature and sea ice thickness is maintained. (Note, however, the magnitude of the flux is independent of the anomaly of sea surface temperature that can develop during a model integration.) See section 4 of Manabe et al. (1991) for a more detailed description of this model.

A quasi-equilibrium climate is obtained by averaging the last 10 years of the 40-year integration of the model, which starts from an isothermal initial condition at rest. It is found that 40 years is long enough for the model to reach a statistical equilibrium condition. The time integration is conducted not only for the normal concentration of the atmospheric carbon dioxide, but also for twice the normal concentration. The equilibrium response of the model to the doubling of atmospheric carbon dioxide is evaluated by computing the difference between the two equilibria.

To evaluate the sensitivity of a simulated climate and its CO_2-induced change to the computational resolution of the model, two versions of the model are used. The first version has the rhomboidal 15 (R15) spectral resolution, which is the resolution of the coupled ocean–atmosphere model used in the present study. The second version has a rhomboidal 30 (R30) resolution, which is twice as high as the first version. It assumes the equilibrium sea surface temperature

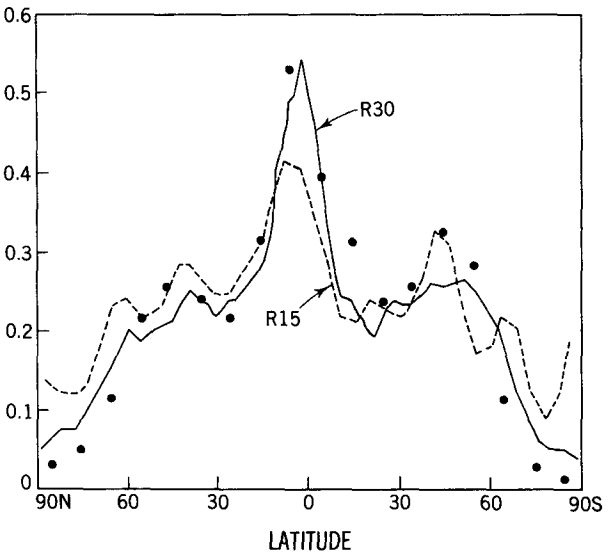

FIG. A1. Latitudinal profiles of zonally averaged, annual mean precipitation rate from the R15 (dashed line) and R30 (solid line) versions of an atmosphere–mixed layer ocean model with the normal CO_2 concentration. The estimates of zonally averaged, actual precipitation rate obtained by Budyko (1963) are indicated by dots. Units are cm day^{-1}.

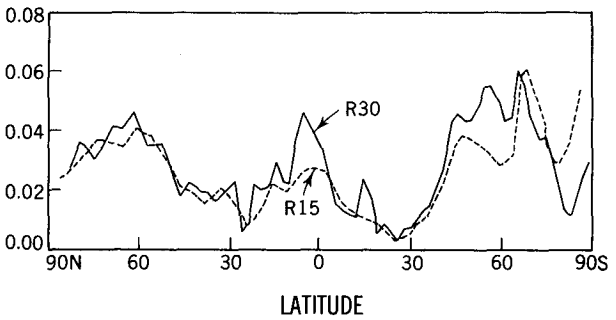

FIG. A2. Latitudinal profiles of the annual mean difference in precipitation rate between the two quasi equilibria of an atmosphere-mixed layer ocean model with normal and twice the normal concentrations of the atmospheric carbon dioxide. Solid line: R30 version. Dashed line: R15 version. Units are cm day^{-1}.

distributions from the R15 model as lower boundary conditions for both integrations with the normal and twice the normal CO_2 concentrations. By comparing the CO_2-induced changes from these two versions of the model, the impact of the model resolution is evaluated.

Figure A1 illustrates the latitudinal profiles of zonal mean precipitation rate from the R15 and R30 versions of the model with the normal CO_2 concentration. In addition, the estimates of the actual precipitation rate obtained by Budyko (1963) are plotted in the same figure for comparison. This figure clearly indicates that the R15 version substantially overestimates the precipitation in high latitudes of both hemispheres. The exact reason for this overestimate has not been determined. We speculate, however, that it results from a fictitious poleward transport of water vapor in the model atmosphere resulting from the spectral truncation of the horizontal moisture field. Fortunately, the bias of the model is reduced significantly when the model resolution is improved from the R15 to the R30 version. In view of the enormous difficulty in estimating the actual rate of precipitation in high latitudes, particularly over oceans, we found the results from the R30 version of the model to be encouraging.

The equilibrium response of the simulated precipitation to a doubling of atmospheric carbon dioxide is shown for the two model resolutions in Fig. A2. Despite the significant difference in precipitation rate in the control experiments, the CO_2-induced change in high-latitude precipitation is very similar between the two versions of the model. These results appear to suggest that the precipitation change of the R15 coupled ocean–atmosphere model in response to a gradual increase of atmospheric CO_2 may not be exaggerated too much, contrary to what was speculated earlier by Manabe et al. (1991).

REFERENCES

Broccoli, A. J., and S. Manabe, 1993: Climate model studies of interactions between ice sheets and the atmosphere–ocean system. NATO Proceedings, *Ice in the Climate System,* Springer-Verlag, in press.

Broecker, W. S., 1987: Unpleasant surprises in the greenhouse? *Nature,* **328,** 123–126.

Bryan, K., 1969: Climate and ocean circulation. Part II: The ocean model. *Mon. Wea. Rev.,* **97,** 828–829.

——, 1987: Potential vorticity in models of the ocean circulation. *Quart. J. Roy. Meteor. Soc.,* **113,** 713–734.

——, and W. W. Hsieh, 1993: The steric component of sea level rise associated with greenhouse warming: A model study. *J. Phys. Oceanogr.,* submitted

——, and L. J. Lewis, 1979: A water mass model of the world oceans. *J. Geophys. Res.,* **84,** 2503–2517.

——, and M. J. Spelman, 1985: The ocean's response to a carbon dioxide-induced warming. *J. Geophys. Res.,* **90**(C6), 11 679–11 688.

——, S. Manabe, and R. C. Pacanowski, 1975: A global ocean–atmosphere climate model. Part II: The oceanic circulation. *J. Phys. Oceanogr.,* **5,** 30–46.

——, ——, and M. J. Spelman, 1988: Interhemispheric asymmetry in the transient response of a coupled ocean-atmosphere model to a CO_2 forcing. *J. Phys. Oceanogr.,* **18,** 851–867.

——, F. G. Komro, S. Manabe, and M. J. Spelman, 1982: Transient climate response to increasing atmospheric carbon dioxide. *Science,* **215,** 56–58.

Crowly, T. J., and G. N. North, 1991: Paleoclimatology. *Oxford Monograph on Geology and Geophysics,* **16,** 339 pp.

Cubasch, U., K. Hasselman, H. Höch, E. Maier-Reimer, U. Mikolajewicz, B. D. Santer, and R. Sausen, 1992: Time-dependent greenhouse warming computations with a coupled ocean–atmosphere model. *Climate Dyn.,* **8,** 55–69.

Delworth, T., S. Manabe, and R. J. Stouffer, 1993: Interdecadal variations of the thermohaline circulation in a coupled ocean–atmosphere model. *J. Climate,* **6,** 1993–2011.

Gordon, C. T., and W. Stern, 1982: A description of the GFDL Global Spectral Model. *Mon. Wea. Rev.,* **110,** 625–644.

Intergovernmental Panel on Climate Change, 1990: Climate Change: The IPCC Scientific Assessment. J. T. Houghton, G. J. Jenkins and J. J. Ephraums, Eds., Cambridge Univ. Press, 366 pp.

Levitus, S., 1982: *Climatological Atlas of the World Ocean.* NOAA Prof. Paper No. 13, U.S. Dept. of Commerce, Washington, D.C., 173 pp.

Manabe, S., 1969: Climate and the ocean circulation: I. The atmospheric circulation and the hydrology of the earth's surface. *Mon. Wea. Rev.,* **97,** 739–744.

——, and A. J. Broccoli, 1985: The influence of continental ice sheets on the climate of an ice age. *J. Geophys. Res.,* **90,** 2, 167–190.

——, and R. J. Stouffer, 1988: Two stable equilibria of a coupled ocean–atmosphere model. *J. Climate,* **1,** 841–866.

——, and ——, 1993: Century-scale effects of increased atmospheric CO_2 on the ocean-atmosphere system. *Nature,* **364,** 215–218.

——, K. Bryan, and M. J. Spelman, 1990: Transient response of a global ocean-atmosphere model to a doubling of atmospheric carbon dioxide. *J. Phys. Oceanogr.,* **20,** 722–749.

——, R. J. Stouffer, M. J. Spelman, and K. Bryan, 1991: Transient response of a coupled ocean–atmosphere model to gradual changes of atmospheric CO_2. Part I: Annual mean response. *J. Climate,* **4,** 785–818.

——, M. J. Spelman, and R. J. Stouffer, 1992: Transient response of a coupled ocean–atmosphere model to gradual changes of atmospheric CO_2. Part II: Seasonal response. *J. Climate,* **5,** 105–126.

Marotzke, J., and J. Willebrand, 1991: Multiple equilibria of the global thermohaline circulation. *J. Phys. Oceanogr.,* **21,** 1470–1493.

Neuman, G., and W. J. Pierson, Jr., 1966: *Principle of Physical Oceanography.* Prentice-Hall, Inc., 545 pp.

Orszag, S. A., 1970: Transform method for calculating vector-coupled sums: Application to the spectral form of the vorticity equation. *J. Atmos. Sci.,* **27,** 890–895.

Schlesinger, M. E., W. L. Gates, and Y. J. Han, 1985: The role of the ocean in a CO_2-induced climatic warming: Preliminary results from the OSU coupled atmosphere–ocean GCM. *Coupled Ocean-Atmosphere Models,* J. C. J. Nihoul, Ed., Elsevier, 447–478.

Spelman, M. J., and S. Manabe, 1984: Influence of oceanic heat transport upon the sensitivity of a model climate. *J. Geophys. Res.*, **89,** 571–586.

Stouffer, R. J., S. Manabe and K. Bryan, 1989: Interhemispheric asymmetry in climate response to a gradual increase of atmospheric CO_2. *Nature,* **342,** 660–662.

Toggweiler, J. R., and B. Samuels, 1993: Is the magnitude of the deep outflow from the Atlantic Ocean actually governed by Southern Hemisphere winds? *The Global Carbon Cycle.* M. Heimann, Ed., Nato ASI Series, Springer-Verlag, 303–331.

Walker, J. C. G., and J. F. Kasting, 1992: Effect of fuel and forest conservation on future levels of atmospheric carbon dioxide. *Paleooceanogr., Paleoclimatol., Paleoecol.,* **97,** 151–189.

Washington, W. M., and G. A. Meehl, 1989: Climate sensitivity due to increased CO_2: Experiments with a coupled atmosphere and ocean general circulation model. *Climate Dyn.,* **4,** 1–38.

Weaver, A. J., and E. S. Sarachik, 1991: The role of mixed boundary conditions in numerical models of the ocean's climate. *J. Phys. Oceanogr.,* **21,** 1470–1493.

Zhang, S., R. J. Greatbatch and C. A. Lin, 1993: A re-examination of the polar halocline catastrophe and implications for coupled ocean-atmosphere modeling. *J. Phys. Oceanogr.,* **23,** 287–299.